16TH EUROPEAN CONFERENCE ON EARTHQUAKE ENGINEERING THESSALONIKI 18 - 21 JUNE 2018

DOES THE ANGLE OF SEISMIC INCIDENCE AFFECT INELASTIC SEISMIC DEMAND? A PROBABILISTIC POINT OF VIEW

Despoina SKOULIDOU[1], Nuno PEREIRA[2], Xavier ROMÃO[3]

ABSTRACT

Probabilistic analysis allows taking into account uncertainties that deterministic approaches usually don't permit. In this context, the uncertainty of the angle of seismic incidence is addressed and its effect on the seismic demand of buildings is examined in a probabilistic framework. Buildings comprising different configurations in-plan and in-elevation are subjected to nonlinear time history analysis with forty bi-directional ground motions. The ground motions are applied along twelve angles of incidence, which are sampled from a uniform distribution, and are further re-sampled into groups of different sizes. The seismic demand distributions of samples derived from different ground motion group sizes applied along different number of angles of incidence are compared to the demand distribution of the reference case considered to be the true demand distribution. The results show that considering more than one angle of seismic incidence always improves the result. The effect of the angle seems to be dependent on the size of the ground motion group and, from a probabilistic point of view, considering more than five angles of incidence has no significant effect on the seismic demand.

Keywords: Angle of seismic incidence; probabilistic seismic demand; RC buildings; statistical measures

1. INTRODUCTION

Several studies performed during the past couple of decades demonstrate the inadequacy of three-dimensional (3D) structural analysis to capture the 'true' seismic demand when only one angle of seismic incidence (ASI) is considered (e.g. see MacRae and Mattheis 2000, Rigato and Medina 2007, Kostinakis et al. 2017, Skoulidou and Romão 2017). The ASI is defined as the angle between the building's structural axes and the direction of the input seismic action, the latter being represented either by two orthogonal response spectra or by a pair of ground motion records. Traditionally, the ASI is assumed to be coincident with the structural axes of the building being analyzed when the latter has two clearly identified perpendicular structural directions (EAK 2003, CEN 2005, NTC 2008). In case of buildings without an easily identified structural configuration, the orientation of the seismic action that should be used to evaluate the seismic safety is not clearly defined in existing standard provisions. Nevertheless, existing literature has shown that considering only one ASI may lead to severely inadequate results, since variations of the seismic demand were shown to reach even 200% between different angles of incidence (Athanatopoulou 2005).

Despite the recognized importance of the ASI in the seismic safety assessment of buildings, analytical expressions for the determination of the effect of the ASI on the structural demand have not yet been developed when dynamic analysis is performed using nonlinear material properties. The development of such expressions or methodologies has been impeded by several factors. Among others, the characteristics of the pair of ground motion records and the ground motion intensity seem to have an important effect since they both affect the inelastic behavior of the structure (Fontara et al. 2015). In addition, structural regularity has also been seen to affect the structural demand (Magliulo et al. 2014).

In this context, the proposed study analyses the uncertainty of structural demand associated to the ASI

[1]PhD student, CONSTRUCT-LESE, Faculty of Engineering, University of Porto, Portugal, dskoulidou@fe.up.pt
[2]PhD student, CONSTRUCT-LESE, Faculty of Engineering, University of Porto, Portugal, nmsp@fe.up.pt
[3]Assistant Professor, CONSTRUCT-LESE, Faculty of Engineering, University of Porto, Portugal, xnr@fe.up.pt

from a probabilistic point of view. Previous probabilistic studies addressing the effect of the ASI can be found for example in Lagaros (2010a) and (2010b), but their focus is on the impact of the ASI on fragility and loss estimations. Instead, the influence of the number of ASIs and of the size of the ground motion pairs on the variability of structural demand distribution is examined herein. The study is carried out considering plan-regular and plan-irregular low- to mid-rise multi-story reinforced concrete (RC) buildings with masonry infilled frame systems. The adequacy of a particular combination of number of ground motion pairs and of ASIs is determined with respect to a reference case that involves forty real ground motion pairs compatible with a conditional mean spectrum and twelve ASIs ranging from 0° to 165° in steps of 15°. All buildings are analyzed for the reference case that also considers different earthquake intensity levels, ranging from elastic to highly inelastic structural response.

2. METHODOLOGY

The aim of the study is to examine the effect of the ASI on the seismic demand of RC buildings from a probabilistic point of view. To achieve this, six benchmark buildings are considered and subjected to nonlinear dynamic analysis for ground motion groups of size 10, 15, 20, 25, 30, 35 and 40 applied along twelve ASIs. Having as a reference the demand obtained for the group of forty ground motions applied along all twelve ASIs, the effectiveness of using different number of ASIs is assessed for the different sizes of the ground motion groups. In the following, the notation n_ASI will be used to refer to the results of a particular size n of ground motions and number of ASIs.
The seismic demand is expressed by the maximum interstory drift ratio (ISD) and the probabilistic analysis is performed on the ISD distributions at distinct intensity levels. A general formulation of the distance between an empirical distribution function $F_n(x)$ and an estimated distribution function $F(x)$ is used to compare the ISD distributions and four statistical measures are employed for this purpose. An illustrative example of the referred demand distributions is shown is Figure 1. The ISD samples correspond to a 20_1 example and the reference 40_12 sample obtained from the 5-story regular building (presented in Section 3.1) and for a seismic intensity equal to 0.44g (explained in Section 3.3).

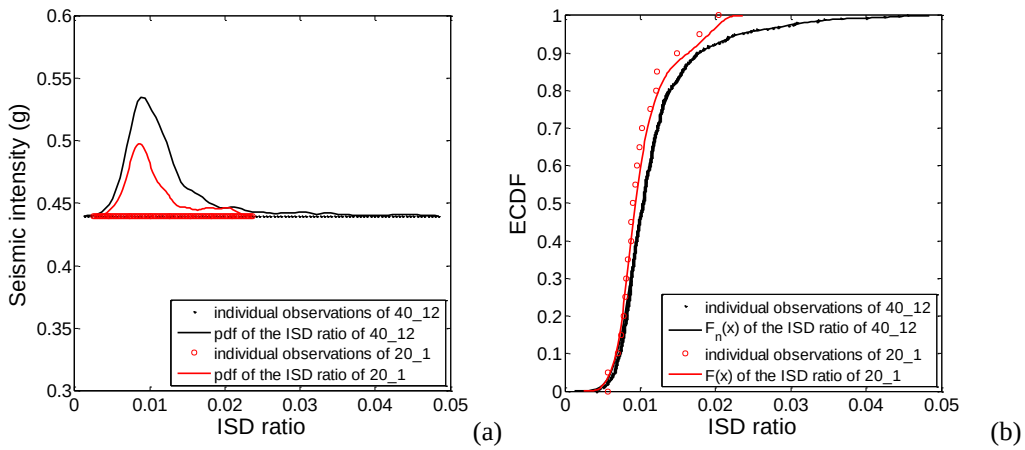

Figure 1. The probability density functions (pdf) (a) and the empirical cumulative distribution functions (ECDFs) (b) of the reference group and a group of n=20 and ASI=1 for an intensity of 0.44g.

The statistical measures correspond to the general form of the well-known Kolmogorov Smirnov (KS_d) (Massey 1951), Kuiper ($Kuiper_d$) (Kuiper 1960), Cramer-von-Mises (CvM_d) (Cramér 1928, von Mises 1928) and Anderson Darling (AD_d) (Anderson and Darling 1954) distances, where the subscript d is used to emphasize the fact that the distance measure is used instead of the formal test statistic. All distances considered are formulated to be more sensitive on specific characteristics of the cumulative distribution functions (CDFs) being compared. KS_d returns the supremum distance between two CDFs and is more sensitive to differences in the median part of the distributions:

$$KS_d = \sup_x \left| F_n(x) - F(x) \right| \quad (1)$$

where sup stands for the supremum operator. $Kuiper_d$ is closely related to the KS_d and returns the sum of the absolute sizes of the most positive and the most negative differences between the two CDFs, thus being equally sensitive to differences in the tails as in the median part of the distribution:

$$Kuiper_d = \max\left[F_n(x) - F(x)\right] + \max\left[F(x) - F_n(x)\right] \quad (2)$$

CvM_d and AD_d are closely related to each other and both belong to the class of quadratic distance measures between CDFs. The former is more akin to the KS_d in the sense that it is more sensitive to differences in the median part of the distributions, whereas the latter places more weight in the tails and is therefore more sensitive to differences in that part of the distributions:

$$CvM_d = \int_0^1 \left[F_n(x) - F(x)\right]^2 dF(x) \quad (3)$$

$$AD_d = \int_0^1 \frac{\left[F_n(x) - F(x)\right]^2}{F(x)\left[1 - F(x)\right]} dF(x) \quad (4)$$

The KS_d and $Kuiper_d$ distances rely only on the maximum deviations of the two CDFs. Consequently, when the two CDFs cross each other multiple times, the maximum deviation decreases, which implies that KS_d and $Kuiper_d$ also reduce. For a more comprehensive analysis of these cases, the CvM_d and AD_d distances are also adopted in this study given their higher sensitivity, since they are expressed as the summation of the squared differences over the total length of the CDFs. As a result, the conclusions deduced from the evolution of CvM_d and AD_d are expected to be more variable than those obtained from the evolution of KS_d and $Kuiper_d$.

3. DETAILS OF THE SELECTED BUILDINGS AND OF STRUCTURAL ANALYSES

3.1 Case studies and structural modeling

Six RC buildings with masonry infilled frame systems are analyzed. The selected buildings have configurations ranging from low- to mid-rise buildings with and without in-plan irregularities. Furthermore, all buildings are located in Lisbon, Portugal and are designed for gravity loads only. The plan view of a typical story of the 3-story irregular (3-Ir), the 4-story irregular (4-Ir) and the 5-story irregular (5-Ir) buildings is presented in Figure 2, along with design details. Similarly, in Figure 3, the plan view of a typical story of the 3-story regular (3-R), the 4-story regular (4-R) and the 5-story regular (5-R) buildings and the design details are also shown. The concrete strength and the yield strength of the reinforcing steel are equal to 25 MPa and 500 MPa, respectively.

All buildings are modeled in the OpenSees computer software (McKenna and Fenves 2011) considering mean values of the material and geometrical properties. A lumped plasticity approach is adopted to simulate the inelastic behavior of all structural elements. Phenomenological hysteresis laws are assigned in rotational springs located on both ends of all columns and beams to simulate inelastic flexural behavior. Two independent springs are assigned to each end of the columns, one for each orthogonal direction, while one spring is assigned to each end of the beams modeling the in-plane flexural behavior. Due to the nature of the selected inelastic modeling approach, no bi-axial moment interaction or axial force moment interaction is considered when modeling the behavior of columns.

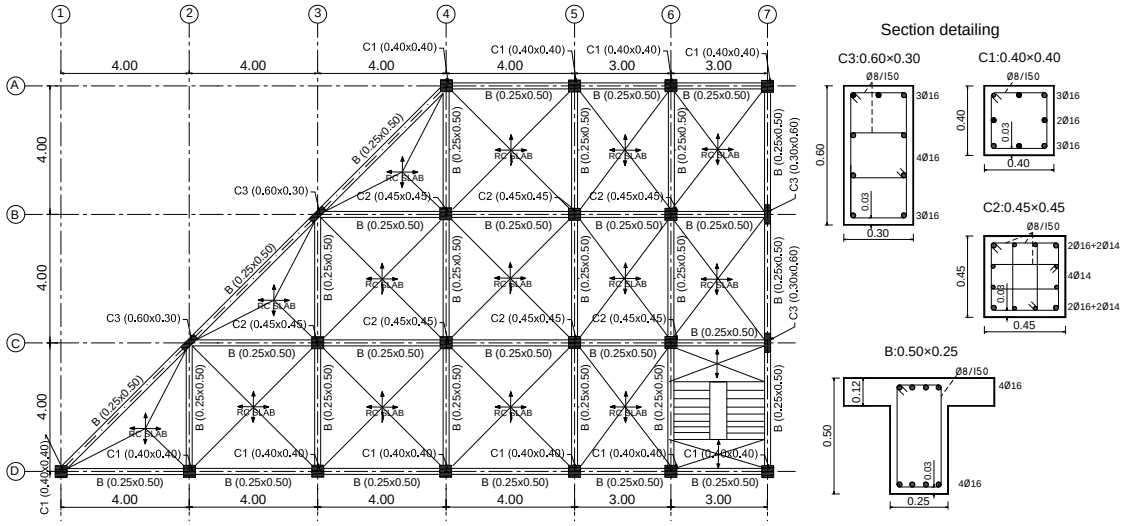

Figure 2. Plan view of a typical story of the 3-Ir, 4-Ir and 5-Ir buildings and design details.

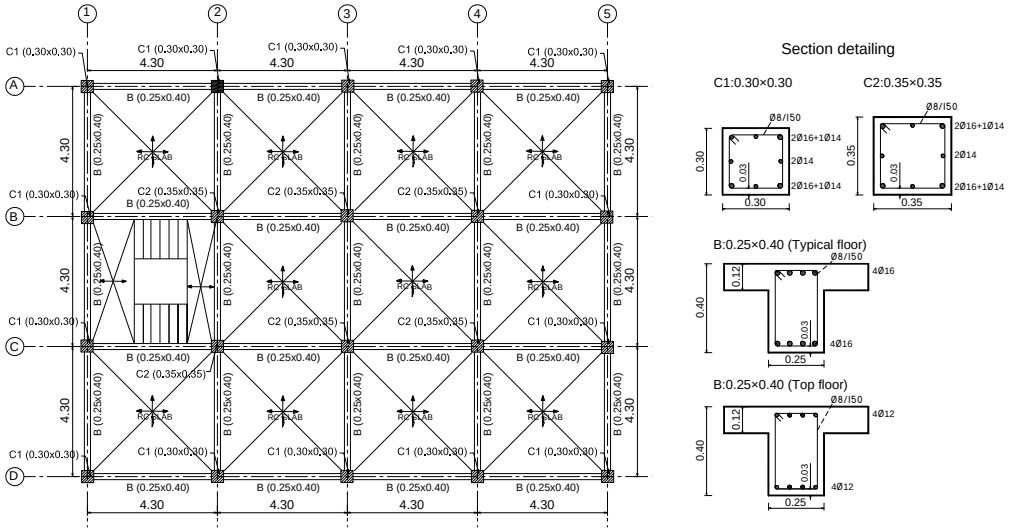

Figure 3. Plan view of a typical story of the 3-R, 4-R and 5-R buildings and design details.

Hysteretic flexural behavior is simulated using the *hysteretic* material provided by OpenSees. The yielding strength (M_y) and the yielding rotation capacity (θ_y) are determined according to Panagiotakos and Fardis (2001). The capping (θ_c) and post-capping rotation (θ_{pc}) capacities are computed according to Haselton et al. (2008) and a final 20% residual strength (M_r) is considered at the ultimate rotation capacity (θ_u) (see the backbone curve in Figure 4(a)). Stiffness, strength and unloading stiffness degradations are considered in the hysteresis curves. Each beam-column element is defined by a serial arrangement of the end springs connected to a linear elastic element. A stiffness modification factor equal to 10 is applied according to Ibarra and Krawinkler (2005) and Zareian and Medina (2010) to account for the effect of the series connection of the elements on the total stiffness of the element. For the beam-column joint, rigid elastic elements are considered with a length equal to half of the length of the corresponding perpendicular element. The possibility of shear failure or beam-column joint failure is not modelled but can be analyzed in post-processing. Infills are considered in all peripheral frames and are modelled using two diagonal compression-only strut elements. The equivalent area of each strut is established based on the maximum lateral force of the infill and on the masonry compressive strength (Dolšek and Fajfar (2008)). The parameters obtained, i.e. the maximum stress (f_m) and strain, are used

to define the masonry material with zero tensile strength simulated by the *Concrete01* constitutive model (Figure 4 (b)). The masonry compressive strength is equal to 3.10 MPa and all infills have a thickness of 0.15m. Additionally, a residual stress equal to 10% of the maximum stress is considered for numerical stability.

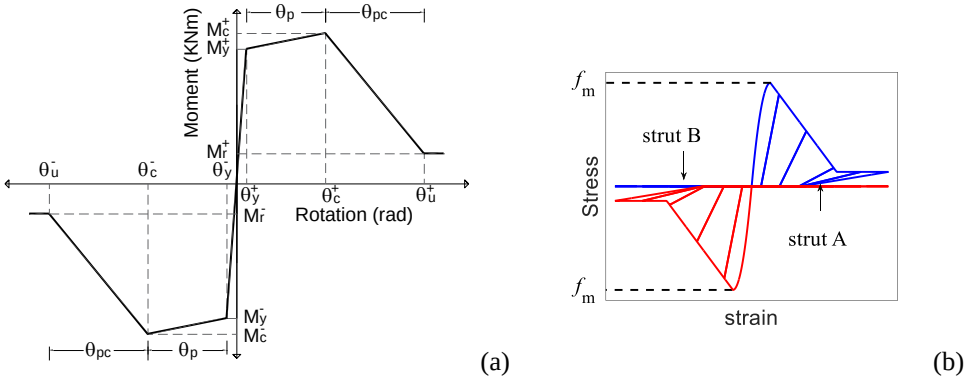

Figure 4. Backbone curve of the Moment-Rotation relationship of all structural elements (a) and cyclic behavior of the strut material of the infills.

A permanent load of 4 kN/m^2 is uniformly distributed on all slabs, additional to the slab self-weight. A uniform live load of 3 kN/m^2 is also assigned to all slabs, except to the top story slabs, where the live load is 1 kN/m^2. Staircases are modeled only as permanent and live loads, which are transferred to the supporting beams and applied uniformly. The corresponding loads are 7.75 kN/m and 8.60 kN/m for the permanent and the live loads, respectively. Masonry infills also load uniformly all peripheral frames with 7 kN/m. The fundamental periods of vibration of each structure are presented in Table 1.

Table 1. First and second mode periods of vibration of the selected buildings.

Periods (s)	**3-R**	**4-R**	**5-R**	**3-Ir**	**4-Ir**	**5-Ir**
T_1,T_2 (w infills)	0.31, 0.25	0.41, 0.31	0.52, 0.39	0.21, 0.15	0.29, 0.20	0.37, 0.26
T_1,T_2 (w/o infills)	0.73, 0.72	0.96, 0.93	1.18, 1.15	0.39, 0.35	0.55, 0.47	0.70, 0.60

3.2 Ground motion selection

The ground motion selection is carried out using the recently developed SelEQ software (Macedo and Castro 2017) considering a conditional mean spectrum (CMS) (Baker 2010) as the target spectrum. The probabilistic seismic hazard analysis of the site is first performed using OpenQuake (Pagani et al. 2014) considering Lisbon, Portugal, as the benchmark site for all structures. Hazard disaggregation is then carried out for four probabilities of exceedance, i.e. 50%, 10%, 5% and 2% in 50 years, at a value of T* for each building. Four CMS are subsequently constructed for each building, each one associated with one of the probabilities of exceedance. The structural period T* corresponds to the average of the first two periods of the building with the infills and the first two periods of the building without the infills (see Table 1). Involving the periods of vibration of the bare structure in the definition of T* is conceptually similar to accounting for the period elongation of the structure after yielding and failure of the infills. Figure 5 shows the four CMS for the 3-R building that has T*=0.5 s.

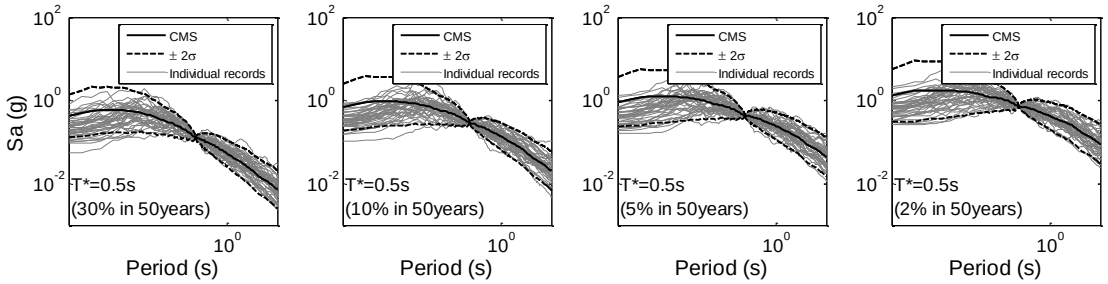

Figure 5. The CMS and the geometric means of the 40 ground motions for the 3-R building.

Ground motion selection is based on a preliminary selection of ground motions from the NGA database (Akkar et al. 2014) based on seismological and strong motion parameters. Subsequently, using the CMS as a target spectrum, 40 bi-directional ground motion records are selected implementing the criteria and the objective function described in Macedo and Castro (2017). As a result, four groups of 40 bi-directional ground motions are obtained for each building, one for each CMS corresponding to the previously referred probabilities of exceedance of 50%, 10%, 5% and 2% in 50 years, e.g. see Figure 5 for the 3-R building and T*=0.5 s.

Each group of 40 bi-directional records is subsequently re-sampled to create groups of size n = 10, 15, 20, 25, 30 and 35. Specific provisions are considered to maintain the compatibility between each new group and the reference group of size 40 in terms of seismic input. As a result, a total number of 100 groups are obtained for each size n.

3.3 Probabilistic demand model and uncertainty considerations

The six buildings presented in Section 3.1 are subjected to multi-stripe analysis (MSA) (Jalayer and Cornell 2009) with the ground motion groups defined in Section 3.2. Following a procedure similar to the one proposed by Christovasilis et al. (2014), the four groups, corresponding to the intensities associated to the previously referred probabilities of exceedance, are scaled up and down to cover a total of fifteen intensities. Figure 6 shows a schematic representation of the scaled average geometric response spectra for the case of the 3-R building (T*=0.5s) and the corresponding scale factors.

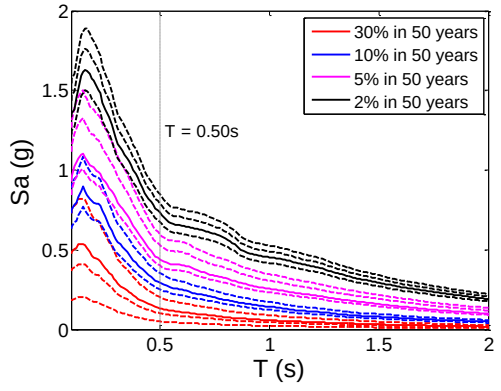

Probability of exceedance	Scale factor	Sa(T*=0.5) (g)
30% in 50 years	0.38	0.05
	0.77	0.10
	1.00	0.13
	1.54	0.20
10% in 50 years	0.86	0.25
	1.00	0.29
	1.21	0.35
5% in 50 years	0.91	0.40
	1.00	0.44
	1.20	0.53
	1.36	0.60
2% in 50 years	0.92	0.67
	1.00	0.73
	1.08	0.79
	1.16	0.85

Figure 6. Average geometric response spectra of the 40 ground motions for different intensities (left) and the scale factors (right) for the 3-R building (T*=0.5s).

All six buildings are subsequently subjected to nonlinear time history analyses for the fifteen intensity levels (stripes) with the 40 record pairs of each stripe applied along twelve ASIs. The considered ASIs range from 0° to 165° in steps 15° and are considered to be equally likely. The sources of uncertainty

considered in the structural response are therefore the result of the record-to-record variability and the ASI of each record. As referred in Section 3.2, 100 groups of ground motions are created for each size n of ground motions to take into account the record-to-record variability in different group sizes. All groups are also applied along different number of ASIs, from one to twelve. The ASIs are sampled from a uniform distribution and a total of 100 combinations of ASIs of size one to eleven are considered. Table 2 summarizes the analyzed cases.

Table 2. Analyzed cases (gr. stands for groups).

ASI \ n	10	15	20	25	30	35	40
1 (100 samples)	100 gr.	100 gr.	100 gr.	100 gr.	100 gr.	100 gr.	1 gr.
2 (100 samples)	100 gr.	100 gr.	100 gr.	100 gr.	100 gr.	100 gr.	1 gr.
…	…	…	…	…	…	…	…
11 (100 samples)	100 gr.	100 gr.	100 gr.	100 gr.	100 gr.	100 gr.	1 gr.
12 (1 sample)	100 gr.	100 gr.	100 gr.	100 gr.	100 gr.	100 gr.	1 gr.

4. RESULTS AND DISCUSSION

The previously referred distance measures are considered to analyze the closeness of $F_n(x)$ and $F(x)$, where the former corresponds to the ECDF of 40_12 for a given intensity level and the latter is the ECDF of each sample at the same intensity level. The average values of each distance obtained for each building are presented in
Figure 7 to Figure 12 (average of the 100 groups of records and the 100 samples of ASIs). Due to space limitations, only a few selected results representative of the general trends are shown. As such, the presented results are for three different intensity levels (one that corresponds to the elastic range of the response, one that corresponds to an intensity where both elastic and inelastic behavior is observed, and one where the response is mostly inelastic). These results are normalized to the maximum distance of each measure, which is always observed for 10_1. The KS_d results are presented with the $Kuiper_d$ results since both measure the maximum vertical distance between the two functions. Similarly, the CvM_d and AD_d are presented together since they are both quadratic distance measures involving the whole sample.

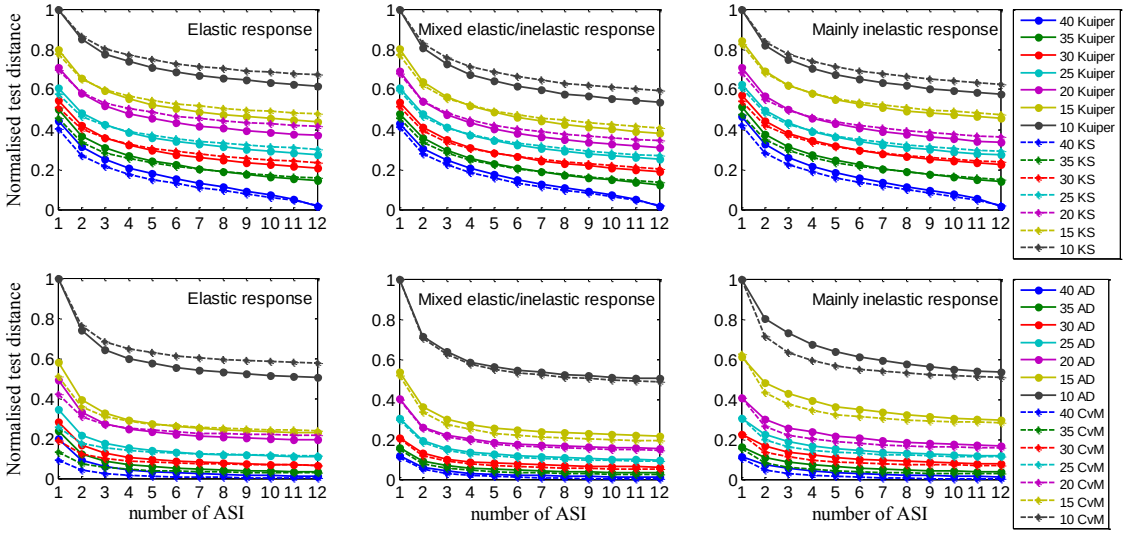

Figure 7. Normalized average distances for the 3-R building.

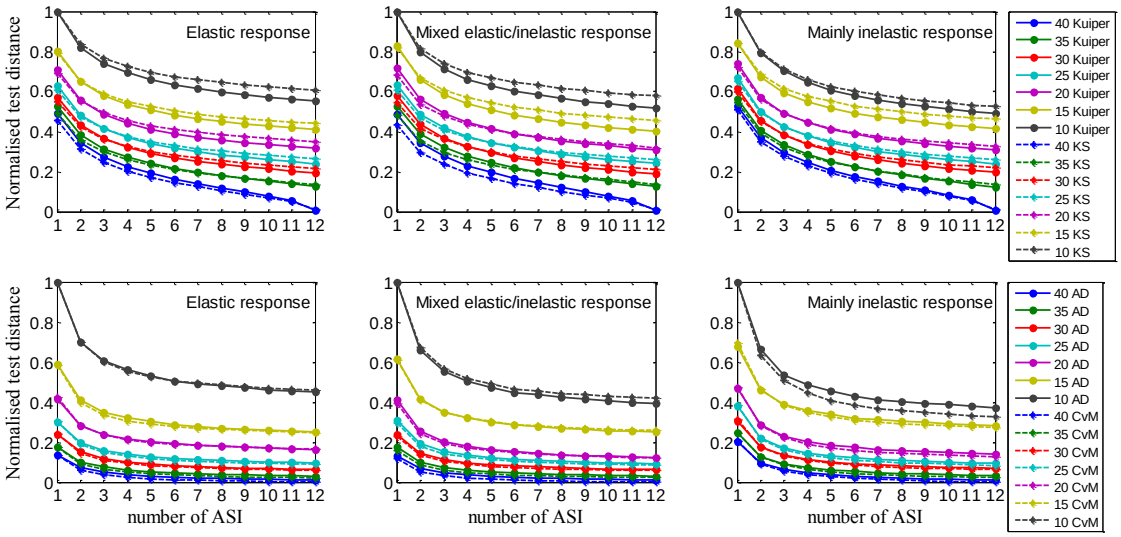

Figure 8. Normalized average distances for the 4-R building.

All distance measures show that, by increasing the number of ASIs, the distance to the reference case decreases for all buildings, all sizes n and all intensity levels. Hence, the results improve when more than 1 ASIs are considered in nonlinear dynamic analysis. However, depending on the size n, the distance decreases up to a certain level and the rate of decrease reduces significantly after considering 3 or 4 ASIs. On this respect, it is observed that using more than 5 ASIs has no remarkable effects on the probabilistic seismic demand for all buildings and all intensity levels that are analyzed. The size n of the ground motion group, on the other hand, appears to have a more pronounced effect on the results and can lead to larger reductions of the statistical distance, while requiring a lower number of analyses. The ASI seems to have a higher effect on the elastic response of the irregular buildings (see Figure 10 to Figure 12) and on the inelastic response of the regular buildings (see
Figure 7 to Figure 9), while the opposite effect stands true for the effect of the ground motion group size.

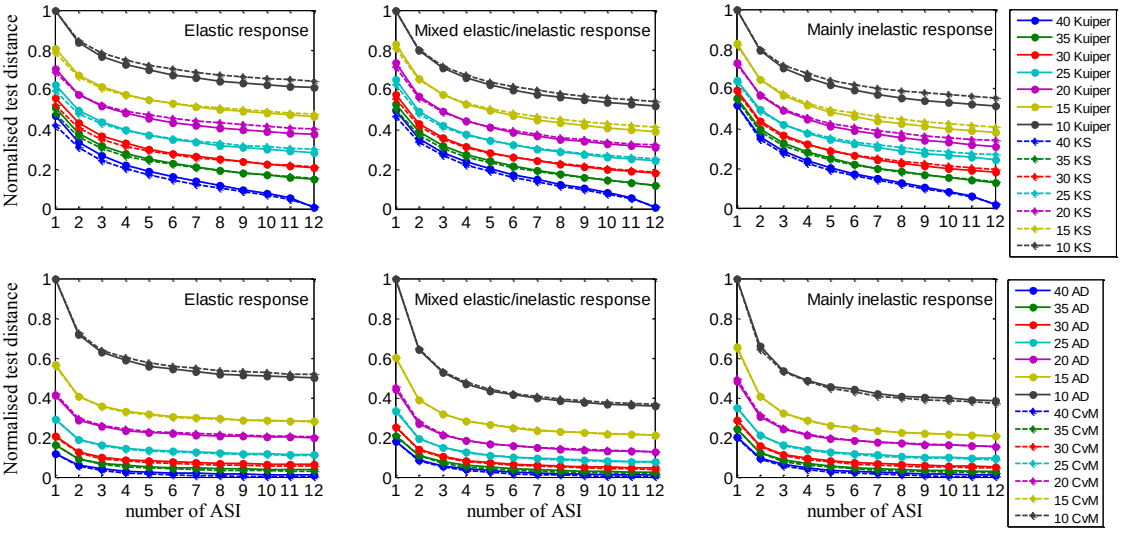

Figure 9. Normalized average distances for the 5-R building.

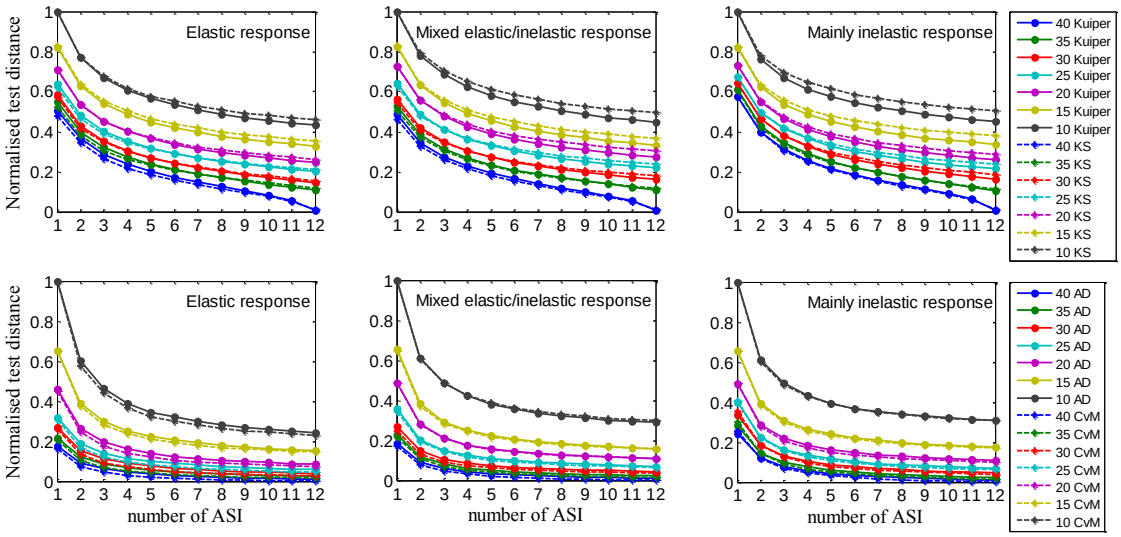

Figure 10. Normalized average distances for the 3-Ir building.

Some more specific remarks can be made by comparing the results of the distance measures in pairs. Starting from the first row of
Figure 7 to Figure 12, the larger decrease of $Kuiper_d$ when compared to KS_d when increasing the number of ASIs indicates that the ASI has a higher effect on the tails of the distribution. The latter observation appears to hold true for all structures and intensity levels (i.e. levels of inelastic behavior), except for the 4-Ir building and for the lower level of inelasticity in which both $Kuiper_d$ and KS_d evolve in the same fashion. Based on the same tests, the opposite trend is observed with the increase of the size n. This higher reduction of KS_d when compared to $Kuiper_d$ suggests that increasing the size n influences more the middle part of the distributions.

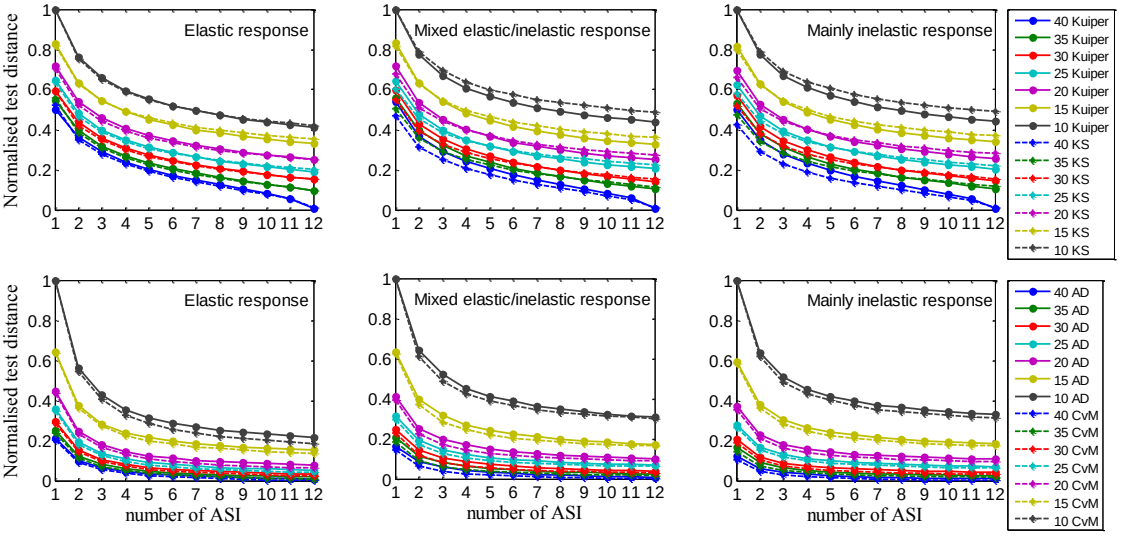

Figure 11. Normalized average distances for the 4-Ir building.

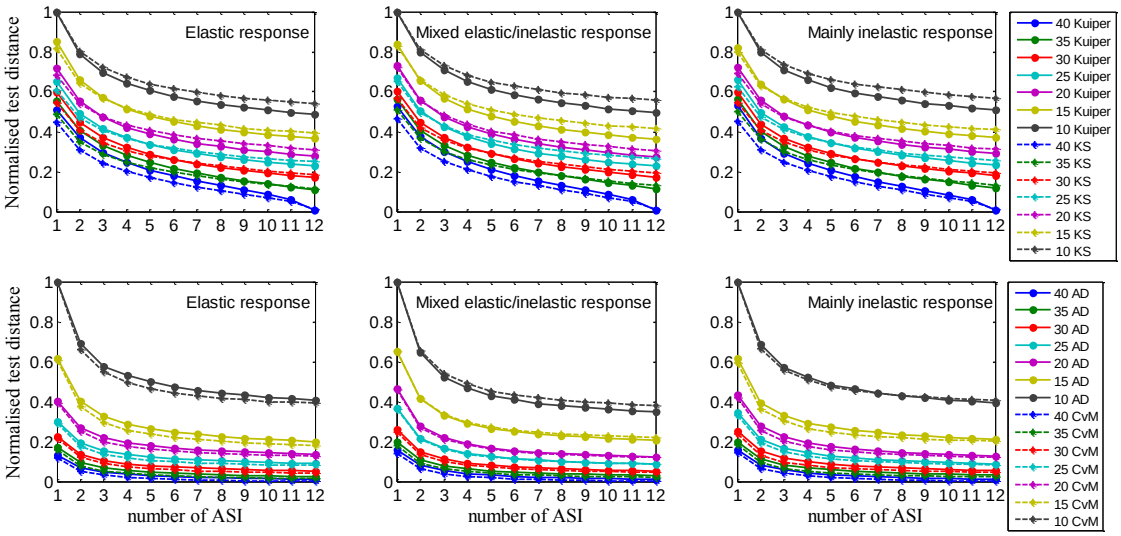

Figure 12. Normalized average distances for the 5-Ir building.

Findings for the quadratic distance measures, shown in the second row of
Figure 7 to Figure 12, are much more variable for different buildings and for different levels of inelasticity. This larger discrepancy of the results was expected given the formulation of the measures. In some cases, e.g. see
Figure 7 for the elastic response, AD_d decreases faster than CvM_d with the ASI, leading to the same conclusions obtained for KS_d and $Kuiper_d$. However, in other cases, e.g. see
Figure 7 and the mainly inelastic response, the opposite trend is observed, with CvM_d reducing faster than AD_d with the increase of ASI. Cases in which both tests decrease simultaneously can also be found, e.g. see Figure 10. Furthermore, no remarkable differences are observed between AD_d and CvM_d when increasing the size n, except for the 3-R building and the elastic response (
Figure 7). Given the small deviations between the results of the two quadratic distances, it can be said that generally AD_d and CvM_d evolve in the same fashion and that no significant weight is given to the tails nor to the middle of the distributions when more ASIs or more ground motions are considered.

5. CONCLUSIONS

The influence of the ASI on the probabilistic seismic demand of six RC buildings is examined. Seismic demand is analyzed for various levels of response, ranging from purely elastic to highly inelastic. The comparison of the seismic demand is carried out at distinct intensity levels for all buildings using four statistical distance measures. The distances that are computed correspond to the distance between the ECDFs of the reference case of 40_12 and cases of different n and number of ASIs.
The distance measures show that considering more than 1 ASI always improves the results, i.e. decreases the distance between the ECDF of a given case and the reference case. The rate of improvement decreases with the increase of the number of ASIs and depends on the size of the group of ground motions. Considering more than 5 ASIs appears to have no significant effect on the probabilistic seismic demand.
The differences between the KS_d and $Kuiper_d$ distance measures suggest that the number of ASIs has a slightly higher effect at the tails of the demand distribution. This effect is sometimes confirmed and sometimes contradicted when analyzing the results obtained by the AD_d and CvM_d distance measures. However, this discrepancy and variability between the results might be justified by the fact that the formulation of these tests involves the summation of the squared differences between the ECDFs under comparison.
Only small differences can be observed between regular and irregular buildings with respect to the effect of the ASI. Still, for regular buildings, it appears that increasing the number of ASIs has a larger effect

on the inelastic range of response, shown by the faster reduction of the distance measures with the increase of the ASI when compared to the one observed for the elastic response. On the other hand, for irregular buildings, a faster decrease of the distance measures with the increase of the ASI is observed for lower seismic intensities.
Finally, both the number of ASIs and ground motion size n contribute to improve the results, i.e. to reduce the distance between the ECDF of given case and the reference one. A trade-off between the optimal number of ASIs and of the size n, based both on computational costs and the accuracy of the obtained results will be the focus of future research.

6. ACKNOWLEDGMENTS

The first author would like to acknowledge the financial support from the Foundation of Science and Technology (FCT) of Portugal through the grant PD/BD/113681/2015. The authors would also like to acknowledge the assistance of Luis Macedo who provided the seismic hazard results and the ground motion records.

7. REFERENCES

Akkar S, Sandıkkaya MA, Şenyurt M, Sisi AA, Ay BÖ, Traversa P, Douglas J, Cotton F, Luzi L, Hernandez B, Godey S (2014). Reference database for seismic ground-motion in Europe (RESORCE). *Bulletin of earthquake engineering*, 12(1): 311-339.

Anderson TW, Darling DA (1954). A Test of Goodness-of-Fit. *Journal of the American Statistical Association*, 49: 765–769.

Athanatopoulou AM (2005). Critical orientation of three correlated seismic components. *Engineering Structures*, 27(2): 301-312.

Baker JW (2010). Conditional mean spectrum: Tool for ground-motion selection. *Journal of Structural Engineering*, 137(3): 322-331.

Christovasilis IP, Cimellaro GP, Barani S, Foti S (2014). On the selection and scaling of ground motions for fragility analysis of structures. *Proceedings of the 2nd European Conference on Earthquake Engineering and Seismology*, 24-29 August, Istanbul, Turkey.

Cramér H (1928). On the composition of elementary errors: First paper: Mathematical deductions. *Scandinavian Actuarial Journal*, 1928(1): 13-74.

Dolšek M, Fajfar P (2008). The effect of masonry infills on the seismic response of a four-storey reinforced concrete frame - a deterministic assessment. *Engineering Structures*, 30(7): 1991-2001.

Fontara IKM, Kostinakis KG, Manoukas GE, Athanatopoulou AM (2015). Parameters affecting the seismic response of buildings under bi-directional excitation. *Structural Engineering and Mechanics*, 53(5): 957-979.

Haselton CB, Goulet CA, Mitrani-Reiser J, Beck JL, Deierlein GG, Porter KA, Taciroglu E (2008). An assessment to benchmark the seismic performance of a code-conforming reinforced-concrete moment-frame building. *Pacific Earthquake Engineering Research Center*, (2007/1).

Ibarra LF, Krawinkler H (2005). Global collapse of frame structures under seismic excitations. Berkeley, CA: *Pacific Earthquake Engineering Research Center*.

Jalayer F, Cornell CA (2009). Alternative non-linear demand estimation methods for probability-based seismic assessments. *Earthquake Engineering & Structural Dynamics*, 38(8): 951-972.

Kostinakis KG, Manoukas GE, Athanatopoulou AM (2017). Influence of seismic incident angle on response of symmetric in plan buildings. *KSCE Journal of Civil Engineering*, 1-11.

Kuiper NH (1960). Tests concerning random points on a circle. *Proceedings of the Koninklijke Nederlandse Akademie van Wetenschappen*, Series A. 63: 38–47

Lagaros ND (2010a). Multicomponent incremental dynamic analysis considering variable incident angle. *Structure and Infrastructure Engineering*, 6(1-2): 77-94.

Lagaros ND (2010b). The impact of the earthquake incident angle on the seismic loss estimation. *Engineering Structures*, 32(6): 1577-1589.

Macedo L, Castro JM (2017). SelEQ: An advanced ground motion record selection and scaling framework. *Advances in Engineering Software*. 114 (2017): 32–47.

MacRae GA, Mattheis J (2000). Three-dimensional steel building response to near-fault motions. *Journal of Structural Engineering*, 126(1): 117-126.

Magliulo G, Maddaloni G, Petrone C (2014). Influence of earthquake direction on the seismic response of irregular plan RC frame buildings. *Earthquake Engineering and Engineering Vibration*, 13(2): 243-256.

Massey FJ (1951). The Kolmogorov-Smirnov Test for Goodness of Fit. *Journal of the American Statistical Association*, 46(253):68-78.

McKenna F, Fenves GL (2011). Opensees 2.5.0, Computer Software. UC Berkeley, Berkeley (CA). http://opensees.berkeley.edu

Pagani M, Monelli D, Weatherill G, Danciu L, Crowley H, Silva V, Henshaw P, Butler L, Nastasi M, Panzeri L, Simionato M (2014). OpenQuake engine: an open hazard (and risk) software for the global earthquake model. *Seismological Research Letters*, 85(3): 692-702.

Panagiotakos TB, Fardis MN (2001). Deformations of reinforced concrete members at yielding and ultimate. *Structural Journal*, 98(2): 135-148.

Rigato AB, Medina RA (2007). Influence of angle of incidence on seismic demands for inelastic single-storey structures subjected to bi-directional ground motions. *Engineering Structures*, 29(10): 2593-2601.

Skoulidou D, Romão X (2017). Critical orientation of earthquake loading for building performance assessment using lateral force analysis. *Bulletin of Earthquake Engineering*, 15(12): 5217-5246.

Von Mises RE (1928). Wahrscheinlichkeit, Statistik und Wahrheit. Julius Springer.

Zareian F, Medina RA (2010). A practical method for proper modeling of structural damping in inelastic plane structural systems. *Computers & structures*, 88(1): 45-53.